J Mater Sci: Mater Med (2008) 19:577–582
DOI 10.1007/s10856-007-3004-y

Effect of silicon on the formation of silk fibroin/calcium phosphate composite

Li Li · Ke-Min Wei · Feng Lin · Xiang-Dong Kong · Ju-Ming Yao

Received: 20 November 2006 / Accepted: 15 March 2007 / Published online: 10 July 2007

Abstract The silk fibroin/calcium phosphate composites were prepared by adding the different amount of Na_2SiO_3 to assess the effect of silicon on the HA (hydroxyapatite) formation in the composites. FTIR and XRD results suggested that the inorganic phase was constituted mainly by the amorphous DCPD (dicalcium phosphate dehydrate), a precursor of HA in the bone mineral, when the composites were prepared at the final Na_2SiO_3 concentration lower than 0.008%. Otherwise, HA was formed as the predominant one in the as-prepared composite, accompanied with a conformational transition in the organic phase of silk fibroin protein from silk I (α-helix and/or polyglycine II (3_1–helix) conformations) to silk II (antiparallel β-sheet conformation). SEM images showed the different morphologies with the samples, i.e., sheet-like crystals in the composites prepared at a low Na_2SiO_3 concentration and rod-like bundles in other composites. The rod-like bundles were connected together to form the porous network, due to the fact that the HA crystals grew with the aggregation of silk fibroin, and further accreted onto the silk fibroin fibrils. TG curves indicated that the composites prepared with a certain amount of additional SiO_3^{2-} had the higher thermal stability because of its high molecular orientation and crystallinity, and high water-holding capacity due to the porous microstructure.

L. Li · F. Lin · J.-M. Yao (✉)
The Key Laboratory of Advanced Textile Materials and Manufacturing Technology of Ministry of Education, College of Materials and Textile, Zhejiang Sci-Tech University, Hangzhou 310018, China
e-mail: yaoj@zstu.edu.cn

K.-M. Wei
Zhejiang Academy of Traditional Chinese Medicine, Hangzhou 310007, China

X.-D. Kong
College of Life Science, Zhejiang Sci-Tech University, Hangzhou 310018, China

Introduction

Hydroxyapatite [HA, $Ca_{10}(PO_4)_6(OH)_2$] is the most commonly used calcium phosphate based biomaterial, which is the major mineral part of natural bones and teeth, due to its excellent biocompatibility, osteoconductivity and bioactivity [1]. However, combination of HA with some biocompatible polymers or proteins was usually used in order to overcome the weak features of HA, i.e., brittleness, insufficient mechanical toughness and tendency of particles to migrate from the implanted sites [2–5]. On the other hand, silk proteins are of practical interest because of their excellent intrinsic properties utilizable in the biotechnological and biomedical fields, such as suture, artificial ligament and substrate for cell culture, as well as the importance of silkworm silks in the manufacture of high-quality textiles [6, 7]. The recent research with silk protein showed its potential application to be explored as hard tissue replacement materials [5, 6].

The human bone is constituted mainly by type I collagen and bone mineral, where the bone mineral has a similar crystalline structure to HA. However, unlike the HA, bone mineral exhibits calcium, phosphate and hydroxyl deficiency, internal crystal disorder [8–10], and contains other substituents, such as carbonate, sodium, magnesium, potassium, zinc, fluorine, chlorine and silicon [8, 10–12]. In 1970s, Carlisle [13, 14] reported that silicon was localized in the active calcification sites in animals, which was from 0.01

to 0.06% in the preosseous border and to 0.12% on the edge of a trabecula. It was also found that silicon deficiency could result in abnormal bone formation and defective cartilaginous tissue [13–16]. Recently, it was reported that the sensitivity of healing response was dependent on the Si level on rate, and an optimal response was obtained at a Si level of 0.8 wt% through its effect on the activity of both bone forming and bone resorbing cells [10]. Silicon also stimulated collagen type I synthesis and osteoblastic differentiation in human osteoblast-like cells in vitro [17]. Moreover, porous silicon had been found to allow fast deposition of HA layers with strong bonds to the surface and good osteointegration when implanted [18, 19]. However, the role of silicon is still unclear in the natural bone formation.

In this study, we prepared the silk fibroin/calcium phosphate composites with or without the additional SiO_3^{2-} ions, and primarily assessed the effect of silicon on the HA formation in the composites through the structural analysis and the properties of silk fibroin/calcium phosphate composite.

Experimental procedure

Preparation of silk fibroin/calcium phosphate composite

Bombyx mori silkworm cocoons were degummed twice with 0.5% (w/v) Na_2CO_3 aqueous solution at 100 °C for 30 min and washed thoroughly with distilled water to remove silk sericin. The fibroin fibers were then dissolved in 9 mol/L LiBr solution at 40 °C for about 30 min, followed by the extensive dialysis against distilled water for 3 days in order to obtain the regenerated silk fibroin solution.

The composites were prepared by adding Na_2SiO_3 (0.12 mol/L) into the silk fibroin solution prior to the addition of $CaCl_2$ (0.2 mol/L) and Na_2HPO_4 (0.2 mol/L) with the Ca^{2+}/HPO_4^{2-} molar ratio of 2.0. The solution was gently stirred and titrated with NaOH solution in drops to keep the pH value at 8.0. The precipitates were collected by centrifugation at 12000 rpm for 10 min and rinsed with deionized water prior to be dried in vacuum. For comparison, the different volume of Na_2SiO_3 solution was added into the silk fibroin solution, which has the final Na_2SiO_3 concentration (w/v) of 0% (denoted as 0Si-SF), 0.007%, 0.008%, 0.01% and 0.10% (denoted as *x*Si-SF, where *x* is 7, 8, 10 or 100), respectively. Na_2CO_3, Na_2SiO_3, $CaCl_2$ and Na_2HPO_4 used here were analytical grade and purchased from Hangzhou Huipu Chemical Agents Co. Ltd., China.

Characterization

Fourier transformed infrared spectroscopy (FTIR): The as-prepared samples were mixed with KBr in the mass ratio of 1:20. FTIR spectra were taken using a Perkin–Elmer Spectrum 1000 apparatus with the wavenumber range of 2000–500 cm^{-1}.

X-ray diffraction (XRD): To investigate the structure and crystallinity of the as-prepared samples, the milled sample powder were analyzed by the X-ray diffraction(XRD) using a Rigaku-D/MAX-2550PC diffractometer equipped for Cu-Kα radiation (λ = 1.5406 Å) in the range of 2θ = 3°–70° with a scanning speed of 0.02°and a count rate of 3.0°/min. The crystallographic parameters of HA were analyzed using MDI JADE 6.5 software.

Scanning electron microscope (SEM): The SEM images of the as-prepared samples were examined on Hitachi Cold-Field Emission SEM S-4700-II scanning electron microscope at 10 KV × 100 K multiples in vacuum.

Thermogravimetric analysis (TGA): The thermal stability of the composites was characterized using a Pyris Diamond TGA thermogravimetric analyzer. The amount of sample for each measurement was about 1 mg, and all of the measurements were carried out under a nitrogen atmosphere and heated up to 500 °C at a heating rate of 10 °C/min. Here, the lyophilized pure silk fibroin powder was used for comparison.

Results and discussion

FTIR spectra

Figure 1 shows the FTIR spectra of different as-prepared silk fibroin/calcium phosphate composites as described above. In the IR spectrum of 0Si-SF (Fig. 1a), the characteristic absorption bands of the amorphous dicalcium phosphate dehydrate (DCPD, Brushite, $CaHPO_4{\cdot}2H_2O$) were observed, a precursor of HA in the bone mineral of inorganic phase. Here, the band centered at 1062 cm^{-1} is assigned to PO_3 symmetrical stretching vibration mode, and the band at 987 cm^{-1} corresponds to P–OH stretching vibration mode. Both are considered to be from the HPO_4^{2-} group of DCPD. However, the inorganic phase also includes some HA composition. Because the bands at 1031 cm^{-1} and 958 cm^{-1} correspond to the P–O stretching vibration modes, and the bands at 602 cm^{-1} and 565 cm^{-1} correspond to the O–P–O bending mode, which are considered to be from the PO_4^{3-} group of HA [20]. The band at 879 cm^{-1} is ascribable to C–O stretching vibration mode on the CO_3^{2-} group, which may be due to the dissolved CO_2 from atmosphere in the solution during agitating. Other three bands at 527 cm^{-1}, 579 cm^{-1} and 789 cm^{-1} may be assigned to the HPO_4^{2-} group too, although both have never been reported previously. Interestingly, no obvious change was observed on the IR spectrum of 7Si-SF (Fig. 1b) prepared with the addition of Na_2SiO_3 solution at the final concentration of 0.007% (w/v). In this work, other two

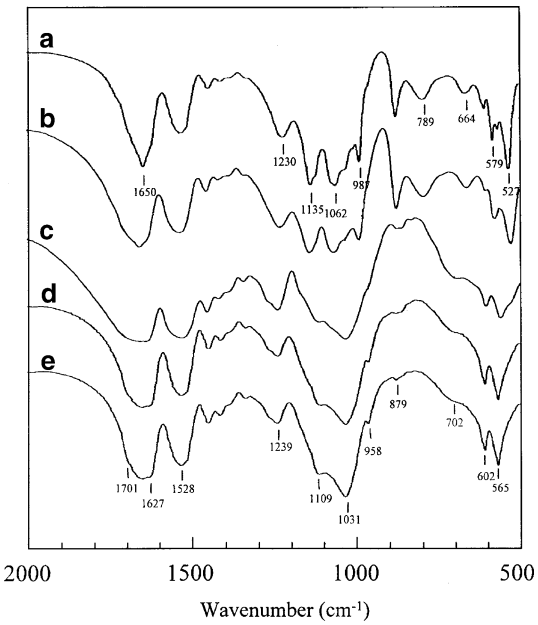

Fig. 1 FTIR spectra of as-prepared silk fibroin/calcium phosphate composites of (**a**) 0Si-SF, (**b**) 7Si-SF, (**c**) 8Si-SF, (**d**) 10Si-SF and (**e**) 100Si-SF

concentrations of 0.005% and 0.006% were also used, and similar spectra were obtained (data not shown).

However, when the final Na_2SiO_3 concentration was increased to 0.008%, a significant change was observed on the IR spectrum, and the spectra of 8Si-SF (Fig. 1c), 10Si-SF (Fig. 1d) and 100Si-SF (Fig. 1e) are almost the same. All of the spectra predominantly show the characteristic absorption bands of HA ($Ca_{10}(PO_4)_6(OH)_2$). The bands at 1109 cm^{-1}, 1031 cm^{-1} and 958 cm^{-1} correspond to the P–O stretching vibration modes, whereas the doublet at 602–565 cm^{-1} corresponds to the O–P–O bending mode. In this system, a certain amount of SiO_3^{2-} in the composite solution can be thought to generate a strong electronegative layer with the pH value increasing due to the abundance of ≡Si-OH^-, and attracted the Ca^{2+} and HPO_4^{2-} from DCPD to form the HA crystals more quickly and easily. Significant difference between two types of spectra is the region between 987 cm^{-1} and 1135 cm^{-1}, where the bands attributed to SiO_3^{2-} vibrations are included leading to the broad peaks in Figs. 1c–e [10].

On the other hand, conformationally sensitive bands for silk fibroin can also be detected in the IR spectra at amide I, II, III and V modes. In the amide I region, the spectra of 0Si-SF and 7Si-SF (Figs. 1a and b) show a sharp peak at 1650 cm^{-1} which is indicative of the presence of silk I structure, i.e., α-helix and/or polyglycine II (3_1–helix) conformations [21, 22]. However, other three spectra of 8Si-SF, 10Si-SF and 100Si-SF (Figs. 1c–e) show the peak shift from 1650 cm^{-1} to 1627 cm^{-1} with the presence of a shoulder at 1701 cm^{-1}, due to the conformational transition from silk I to silk II, i.e., antiparallel β-sheet conformation. Amide I mode represents the C=O stretching. Here, the peaks in the later three spectra of 8Si-SF, 10Si-SF and 100Si-SF are much broad than that in the spectra of 0Si-SF and 7Si-SF, ascribable to carbonyl group which may interact with calcium phosphate more powerful.

Same results can be obtained from amide II and III regions. The amide II and III bands are centered at 1528 cm^{-1} and 1239 cm^{-1}, respectively, in regions of typical β-sheet conformation, where the bands of α-helix and/or polyglycine II (3_1-helix) conformations located at 1528 cm^{-1} and 1230 cm^{-1}. In the low frequency region of the spectra, the bands at 702 cm^{-1} and 664 cm^{-1} are the amide V vibrations due to β-sheet and α-helix conformations, respectively. These spectral features revealed that 0Si-SF and 7Si-SF had a prevalent α-helix and/or polyglycine II (3_1-helix) conformations, and 8Si-SF, 10Si-SF and 100Si-SF had a β-sheet conformation with some contents of α-helix and/or polyglycine II (3_1-helix) conformations remained.

The conformational transition induced by the addition of SiO_3^{2-} was confirmed. Figure 2 shows the expanded amide I and II regions of IR spectra of lyophilized pure silk fibroin powder and 10Si-SF powder without biomineralization. The spectrum of silk fibroin powder (Fig. 2a) shows the 1647 cm^{-1} and 1521 cm^{-1} sharp peaks, while that of 10Si-SF powder without biomineralization (Fig. 2b) shows the peak shift to 1626 cm^{-1} with the presence of a shoulder at 1701 cm^{-1} in amide I region, due to the conformational transition from silk I to silk II, i.e., from α-helix and/or polyglycine II (3_1-helix) to antiparallel β-sheet conformation.

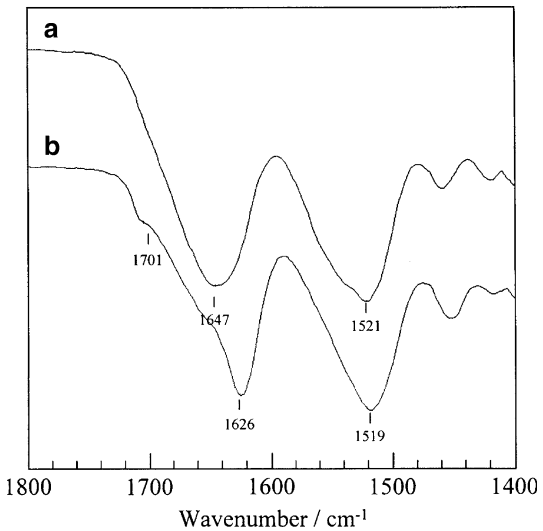

Fig. 2 Expanded FTIR spectra of lyophilized (**a**) pure silk fibroin powder and (**b**) 10Si-SF powder without biomineralization

XRD

Figure 3 shows the XRD patterns of different as-prepared silk fibroin/calcium phosphate composites with the peak assignments. In Figs. 3a and b, the predominant crystalline phase of calcium phosphate is DCPD, with a small content of HA. By the addition of SiO_3^{2-} in the solution to the final concentration of 0.008% (w/v), the HA is the major inorganic phase in the composites, as judging from the characteristic HA diffraction peaks of (211), (002) and (004) planes (Figs. 3c–e), and no DCPD is detected. This result agrees well with above founding from the IR spectra, and suggests that silicon can significantly accelerate the phase transition from DCPD to HA when the Na_2SiO_3 content reaches 0.008% (w/v).

Table 1 indicates that the 10Si-SF and HA are very similar in their crystallographic parameters of lattice constants. Along *c*-axis and *a*-axis, however, their crystallographic parameters significantly differ from each other. Especially from HA to 10Si-SF, the aspect ration, L_c/L_a, increase from 1.37 to 2.72, indicating that the HA crystallites in 10Si-SF composites show more anisotropic growth with higher extent of lattice imperfection along *c*-axis. So that, the peaks assigned to HA in the Figs. 3c–e are apparently broad compared with those to the commercial HA reported previously [2, 24]. The preferential orientation of HA crystallites along *c*-axis is promoted by the certain amount of SiO_3^{2-} treatment to SF. The larger lattice imperfection is thought to be the incorporation of silicon ions into HA structure by replacing calcium ions.

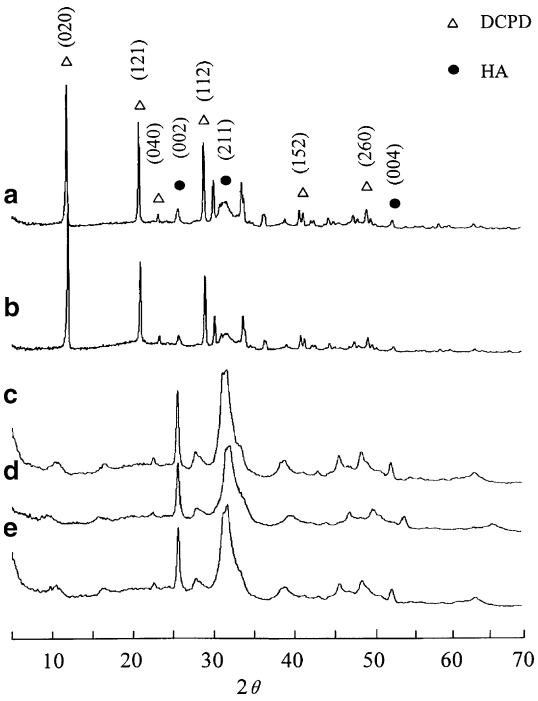

Fig. 3 XRD spectra of as-prepared silk fibroin/calcium phosphate composites of (**a**) 0Si-SF, (**b**) 7Si-SF, (**c**) 8Si-SF, (**d**) 10Si-SF and (**e**) 100Si-SF

Table 1 Crystal size and crystallographic parameters of HA crystals

Samples	L_c [A] (nm)	L_a [A] (nm)	L_c/L_a	*a* (Å)	*c* (Å)
HA[B]	52	38	1.37	9.408	6.876
10Si-SF	220	81	2.72	9.414	6.859

[A] L_c and L_a represents the crystalline size along *c*-axis and *a*-axis, respectively

[B] Data from the International Centre for Diffraction Data (ICDD) (Card No. JCPDS 09–432)

SEM

The SEM images of as-prepared 0Si-SF and 10Si-SF are shown in Fig. 4, where the shape of two samples is significantly different. In Fig. 4a, the 0Si-SF sample takes the irregular sheet-like crystals. However, the rod-like bundles (around 30–50 nm in width) are observed in the 10Si-SF sample with some intimate bonding among them to form the porous network (Fig. 4b). The different features of two samples indicated that there was different interaction between the organic and inorganic phases. In the case of 0Si-SF sample, the inorganic phase is predominantly the DCPD crystals observed as the sheet-like shape, which are formed solely without strong interaction with silk fibroin molecules. In contrast, HA crystals grow with the aggregation of silk protein molecules through the interactions between the Ca^{2+}/PO_4^{3-} and hydrophilic polar groups on the molecular chains. As a result, the HA crystals further accrete onto the silk fibroin fibrils. The 3D porous microstructure formed by the silk fibroin/HA nanocomposites, similar to that of human bone, is very important, which enables the body fluid and blood to enter into the pores so that the further bony metabolism and ingrowth can be promoted in implants [2, 24].

TGA

Figure 5 shows the TGA curves of lyophilized pure silk fibroin powder (a, solid line), 0Si-SF (b, dash line) and 10Si-SF (c, dotted line), respectively, where the silk fibroin powder was reported to take the amorphous structure [25]. Figure 5a presents a typical TGA curve of amorphous silk fibroin [26], where the weight residue starts to decline sharply at 285 °C due to the thermal degradation of protein. However, the decomposition temperature of silk fibroin in 0Si-SF and 10Si-SF are shifted to higher values of 300 °C and 320 °C, respectively, suggesting the high molecular orientation and crystallinity in the silk fibroin proteins, especially in 10Si-SF sample. Same results are

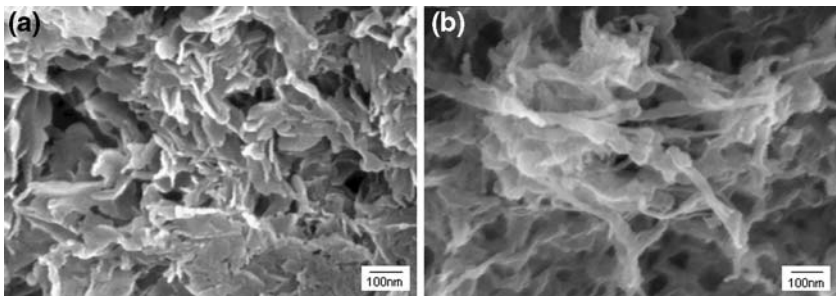

Fig. 4 SEM images of as-prepared silk fibroin/calcium phosphate composites of (**a**) 0Si-SF and (**b**) 10Si-SF

obtained from their weight residue declining rate. At 500 °C, the weight residue is 61.2% for 0Si-SF, while 72.4% for 10Si-SF due to the higher interaction between silk fibroin and HA phase. The initial weight loss of 7.2% at around 100 °C for amorphous silk fibroin powder is due to the evaporation of water. It is noteworthy that the water content and evaporation procedure in 0Si-SF and 10Si-SF samples are significantly different with the pure silk fibroin. The water evaporation in 0Si-SF is constituted by two steps. The initial weight loss of 6.8% at around 100 °C is due to the evaporation of free water in the composites, similar to the pure silk fibroin powder. The weight residue then declined sharply at 122 °C due to the evaporation of bound water, i.e., hydrated water, in DCPD. In this work, the theoretical content of hydrated water in DCPD is 12.2%, which is in agreement with the experimental data observed in Fig. 5b. In the 10Si-SF sample, however, the water evaporation occurred gradually till above 150 °C with a total water content of about 19%, thought to be due to the loosely bound water inside the porous nanocomposites. Moreover, it suggests that the 10Si-SF sample has the high water-holding capacity, which is essential as a biomaterial for cell proliferation.

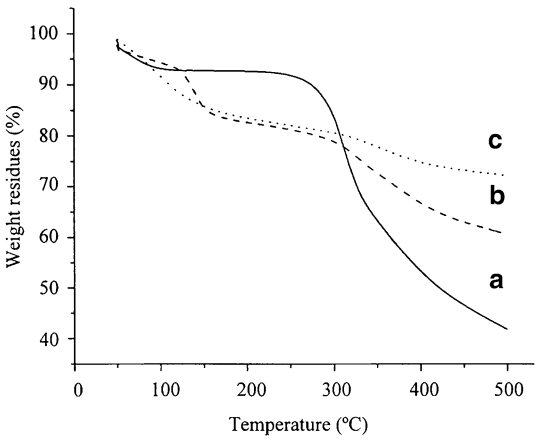

Fig. 5 TGA curves of (**a**) lyophilized pure silk fibroin powder, and the as-prepared silk fibroin/calcium phosphate composites of (**b**) 0Si-SF and (**c**) 10Si-SF

Conclusions

It is well known that HA is the most thermo-dynamically stable calcium phosphate with the high bioactivity. In this work, the FTIR and XRD results showed that the additional silicon could accelerate the HA crystal formation in the silk fibroin/calcium phosphate composite when the final Na_2SiO_3 concentration was higher than 0.007% (w/v). The formed silk fibroin/HA composite had the nano-size, rod-like morphology and porous microstructure, leading to the high water-holding capacity. It although needs more works to clarify the detailed effects of silicon content, initial fibroin solution properties, as well as the reaction conditions and appropriate Ca^{2+}/PO_4^{3-} ratio on the formation of nanocomposite, this funding has provided the evidence that it is possible to regulate the formation, further the properties of calcium phosphate-based biopolymer composites.

Acknowledgements This work was supported by the Program for Changjiang Scholars and Innovative Research Team in University (No. IRT0654), the National Natural Science Foundation of China (No. 20404011 and 10672145) and Zhejiang Natural Science Foundation of China (No. R404066 and Y205468).

References

1. P. DUCHEYNE and Q. QIU, *Biomaterials* **20** (1999) 2287
2. L. WANG, R. NEMOTO and M. SNNA, *J. Nanoparticle Res.* **4** (2002) 535
3. X. D. KONG, F. Z. CUI, X. M. WANG, M. ZHANG and W. ZHANG, *J. Cryst. Growth* **270** (2004) 197
4. M. C. CHANG, T. IKOMA, M. KIKUCHI and J. TANAKA, *J. Mater. Sci. Lett.* **20** (2001) 1199
5. I. YAMAGUCHI, K. TOKUCHI, H. FUKUZAKI, Y. KOYAMA, K. TAKAKUDA, H. MONMA and J. TANAKA, *J. Biomed. Mater. Res.* **55** (2001) 20
6. J. YAO and T. ASAKURA, in *Encyclopedia of Biomaterials and Biomedical Engineering*, edited by G. E. WNEK and G. L. BOWLIN (Marcel Dekker, Inc., New York, 2004) p. 1363
7. G. H. ALTMAN, F. DIAZ, C. JAKUBA, T. CALABRO, R. L. HORAN, J. CHEN, H. LU, J. RICHMOND and D. L. KAPLAN, *Biomaterials* **24** (2003) 401
8. D. McConnel, in "Biologic Apatites" (Springer, Berlin, 1973) p. 68
9. A. S. POSNER, *Physiol. Rev.* **49** (1969) 760
10. K. A. HING, P. A. REVELL, N. SMITH and T. BUCKLAND, *Biomaterials* **27** (2006) 5014

11. R. Z. LEGEROS and J. P. LEGEROS, in *An Introduction to Biocramics*, edited by L. L. HENCH and J. WILSON (World Scientific, Singapore, 1993) p. 139
12. M. O. YAMADA, Y. TOHNO, S. TOHNO, M. UTSUMI, Y. MORIWAKE and G. YAMADA, *Biol. Trace Elem. Res.* **95** (2003) 113
13. E. M. CARLISLE, *Science* **167** (1970) 279
14. E. M. CARLISLE, *Science* **178** (1972) 619
15. K. SCHWARZ and D. B. MILNE, *Nature* **239** (1972) 333
16. A. E. POTER, N. PATEL, J. N. SKEPPER, S. M. BEST and W. BONELD, *Biomaterials* **24** (2003) 4609
17. D. M. REFFITT, N. OGSTON, R. JUGDAOHSINGH, H. F. J. CHEUNG, B. A. J. EVANS, R. P. H. THOMPSON, J. J. POWELL and G. N. HAMPSON, *Bone* **32** (2003) 127
18. H. WEN, Q. LIU, J. WIJN, K. DE GROOT and F. CUI, *J. Mater. Sci.: Mater. Med.* **9** (1998) 121
19. P. FRAYSSINET, F. BRAYE and G. WEBER, *J. Scann. Microsc.* **19** (1997) 253
20. M. J. GLIMCHER, L. C. BONAR, M. D. GRYNPAS, W. J. LANDIS0 and A. H. ROUFOSSE, *J. Cryst. Growth* **53** (1981) 100
21. G. FREDDI, P. MONTI, M. NAGURA, Y. GOTO and M. TSUKADA, *J. Polym. Sci. B: Polym. Phys.* **35** (1997) 841
22. D. WILSON, R. VALUZZI and D. KAPLAN, *Biophys. J.* **78** (2000) 2690
23. X. D. KONG, X. M. WANG, X. YU and F. Z. CUI, *Key Eng. Mater.* **288–289** (2005) 191
24. P. SEPULVEDA, J. G. P. BINNER, S. O. ROGERO, O. Z. HIGA and J. C. BRESSIANI, *J. Biomed. Mater. Res.* **50** (2000) 27
25. T. ASAKURA, A. KUZUHARA, R. TABETA and H. SAITO, *Macromolecules* **18** (1984) 1841
26. M. TSUKADA, M. OBO, H. KATO, G. FREDDI and F. ZANETTI, *J. Appl. Polym. Sci.* **60** (1996) 1619